BMC Cancer

RESEARCH

Open Access

Establishment and characterization of CHC-X1: the third human combined hepatocellular–cholangiocarcinoma cell line

Huan Tang[1†], Changpeng Chai[2,3†], Xin Miao[4†], Yuanhui Su[1], Cheng Yu[1,5], Jianfeng Yi[3,6], Zhengfeng Wang[2,3], Hui Zhang[1,7], Zhenjie Zhao[2,3], Linpei Wang[8,10*], Wence Zhou[1,7,10*] and Hao Xu[2,3,9,10*]

Abstract

Combined hepatocellular-cholangiocarcinoma (cHCC-CCA) represents an uncommon variant of primary liver cancer. In recent years, its incidence rate has increased. Thus, it is essential to perform comprehensive investigations into cHCC-CCA to develop suitable treatment strategies. So far, only two cell lines (CLs) of this cancer type have been reported. More cHCC-CCA CLs need to be established for research purposes. In this investigation, we developed a stable cHCC-CCA CL, named CHC-X1. STR analysis confirmed that CHC-X1 is a new human cHCC-CCA CL. CHC-X1 is a complex karyotype. Its population doubling time is 50.72 h. Under suspended conditions, CHC-X1 can form tumor spheres and organoids in Matrigel. These cells exhibit sensitivity to paclitaxel while demonstrating resistance against oxaliplatin, gemcitabine, and 5-FU. After inoculation into NXG mice, CHC-X1 can quickly form subcutaneous transplant tumors, exhibiting a tumor establishment rate of 67%. Immunohistochemical staining showed that CHC-X1 is a tumor CL with both liver cell differentiation and bile duct cell differentiation characteristics. It may function as a useful model for identifying the origins of cHCC-CCA and the advancement of potential treatments.

Keywords Combined hepatocellular-cholangiocarcinoma, Cell lines, Transplanted tumor, Drug sensitivity, Drug resistance

[†]Huan Tang, Changpeng Chai and Xin Miao contributed equally to this work and share first authorship.

*Correspondence:
Linpei Wang
wlp@fjmu.edu.cn
Wence Zhou
zhouwc129@163.com
Hao Xu
amoyxu@126.com
[1]The Second Clinical Medical School of Lanzhou University, Lanzhou 730000, China
[2]The Fourth Department of General Surgery, The First Hospital of Lanzhou University, Lanzhou 730000, China
[3]The First Clinical Medical School of Lanzhou University, Lanzhou 730000, China
[4]Department of Nephrology, The First Affiliated Hospital of Zhejiang Chinese Medical University, Zhejiang Provincial Hospital of Chinese Medicine, Hangzhou 310006, China
[5]Department of Anesthesiology, Lanzhou University Second Hospital, Lanzhou 730000, China
[6]The First School of Clinical Medicine of Gansu University of Chinese Medicine, Lanzhou 730000, China
[7]Department of General Surgery, Lanzhou University Second Hospital, Lanzhou 730000, China
[8]Department of Hepatobiliary and Pancreatic Surgery, The Second Affiliated Hospital of Fujian Medical University, Quanzhou 362000, China
[9]Department of Hepatobiliary Surgery, The First Affiliated Hospital of Zhejiang Chinese Medical University, Zhejiang Provincial Hospital of Chinese Medicine, Hangzhou, Zhejiang 310006, China
[10]No. 54 Youdian Road, Shangcheng District, Hangzhou, Zhejiang, China

Introduction

Combined hepatocellular-cholangiocarcinoma (cHCC-CCA) is a highly invasive primary liver cancer that exhibits both hepatocyte and bile duct differentiation [1]. This condition is relatively rare, accounting for only 0.77–1.8% of primary liver cancers [2–5]. However, the actual incidence may be higher than reported, as many patients who have not undergone surgery or needle biopsy are often misdiagnosed as having hepatocellular carcinoma or intrahepatic cholangiocarcinoma [2]. cHCC-CCA tends to manifest across various age groups, yet it is predominantly observed in middle-aged and elderly patients, with a male-to-female ratio of roughly 1.9–2.5:1 [2–7]. The overall prognosis of combined hepatocellular- cholangiocarcinoma is poor, and is worse than that of hepatocellular carcinoma. However, its prognosis compared to the prognosis of intrahepatic cholangiocarcinoma is still controversial [2, 3, 8–10]. Radical liver resection is the preferred treatment for cHCC-CCA [2, 8, 11]. However, due to the high invasiveness and high postoperative recurrence rate of the disease, systemic adjuvant therapy is still inevitable for many patients [1, 8]. In addition, due to the rarity of tumors and the lack of clinical trials, standardized adjuvant therapy for cHCC-CCA still needs to be established [1, 12].

Tumor cell lines (CLs) can, to some extent, reflect the characteristics of tumors and are the most widely used models in tumor research. Over the past few decades, tumor CLs have greatly promoted the understanding of tumor biology and helped in the development of antitumor drugs [13–14]. However, only two human cHCC-CCA CLs (KMCH-1 and KMCH-2) have been reported in the literature [15–16], both of which originate from Japanese patients. Therefore, establishing novel cHCC-CCA cellular models is essential for advancing more efficacious therapeutic approaches.

In this investigation, we effectively generated a stable cHCC-CCA CL, named CHC-X1, utilizing tumor tissue surgically excised from an individual with this cancer. CHC-X1 shows promise as a significant experimental model for examining the biological behavior of cHCC-CCA and developing new drugs.

Methodologies and materials

This research was sanctioned by the Medical Ethics Committee of the First Hospital of Lanzhou University (LDYYLL2022-345), and all patients provided written informed consent before enrolment. The experiments involving animals complied with the ARRIVE guidelines and the Guidelines for the Care and Use of Laboratory Animals of China.

The approach utilized in this research parallels techniques utilized in earlier investigations [17–18].

Patient clinical data

The 31-year-old male patient who presented with upper abdominal distension and pain persisting for more than two years on February 28, 2022, in the Fourth Ward of the General Surgery Department at the First Hospital of Lanzhou University. He did not undergo preoperative neoadjuvant chemotherapy or radiation therapy. A left hemihepatectomy was performed on March 9, 2022. The patient had no history of long-term smoking or alcohol consumption, and no chronic diseases like hypertension, diabetes, or coronary heart disease. In addition, there was no history of infectious diseases like hepatitis B and C. Preoperative laboratory examination revealed an alpha fetoprotein level of 9.3 U/mL (reference range: 0–5.8 U/mL), carcinoembryonic antigen at 943.0 ng/mL (0–4.7 ng/mL), and carbohydrate antigen 19 – 9 at 19.9 U/mL (reference range: 0–35 U/mL). Preoperative CT imaging showed uneven enhancement in the liver's left lobe, predominantly in the portal vein phase and not marked in the hepatic artery phase, suggesting a malignant liver tumor (Fig. 1A and B).

Tumor tissue acquisition

After the surgical specimen was excised, it was dissected, revealing pink, diffusely growing new organisms in the left half of the liver (Fig. 1C and D). A 1 cm × 1 cm section of tumor tissue was excised from the edge of the tumor and immediately transferred into a 15-mL centrifuge tube (NEST Scientific) containing transport solution (RPMI-1640 [Gibco] + 1% penicillin–streptomycin [VivaCell]) to the laboratory, ensuring that the transport time did not exceed half an hour. This was followed by tumor cell isolation and primary culture. Two small pieces of tumor tissue were retained: one was frozen at – 80 °C for short tandem repeat (STR) identification, and the other was fixed and preserved in 4% paraformaldehyde (Servicebio) for subsequent H&E staining and immunohistochemical (IHC) staining research. The entire sampling and transportation process was carried out under sterile conditions.

Primary cell isolation and culture

The tumor tissue underwent 3–5 rinses in sterile PBS (Vivacell). In aseptic conditions, it was minutely minced using a scalpel and introduced into a blend of IV collagenase (Gibco) and dispase II (Invitrogen) in RPMI-1640 (Gibco), then agitated at 37 °C for enzymatic dissociation (ED). The liquid fraction was extracted once one-third of the tissue had disintegrated, centrifuged at 400 ×g for 5 min, and removed. The resultant pellet was cleansed with PBS, re-centrifuged, and resuspended in complete culture medium (CCM) 1 (DMEM/F-12 [Gibco] + 10% FBS [VivaCell] + 1% penicillin–streptomycin [VivaCell]). This mixture was then seeded in a six-well plate (NEST)

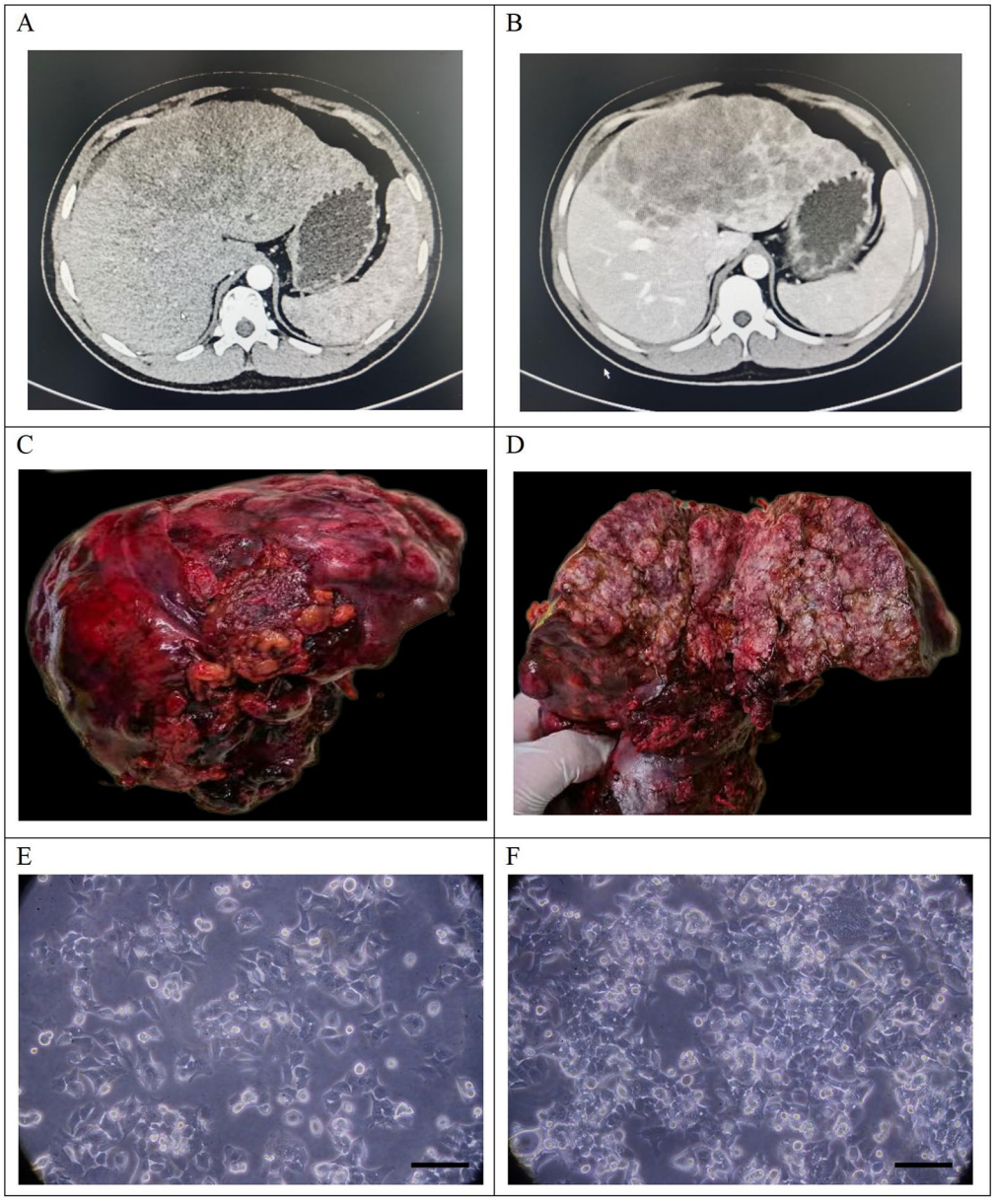

Fig. 1 Clinical data and cell morphology. (**A**–**B**) Preoperative computed tomography image shows a huge lesion in the left liver; (**C**–**D**) Gross examination of the postoperative specimen reveals a pink mass in the left liver; (**E**–**F**): Microscopic examination shows the morphology of CHC-X1 cells under a light microscope (scale bar = 50 μm)

and incubated at 37 °C in a 5% CO_2 atmosphere. The medium was refreshed every 48 h. Fibroblast elimination was achieved through microscope-guided scraping and selective digestion. From the fifth passage onward, cells were split at a 1:2 ratio and cryopreserved in a serum-free rapid freezing medium (Mei5 Biotechnology). Beginning with the 15th passage, CCM 2 (RPMI-1640 [Gibco] + 10% FBS [VivaCell] + 1% penicillin–streptomycin [VivaCell]) was utilized to sustain cell proliferation. Cell growth patterns were routinely monitored and documented using an inverted microscope (Leica, S40 SLIder).

Examination of DNA short tandem repeat sequences

CHC-X1 cells (P26) in the logarithmic growth phase (LGP) were taken, and after ED with 0.25% trypsin (VivaCell), the cells were gathered. Both the cells and the primary tumor tissue were thendispatched to Suzhou Genetic Testing Biotechnology Corporation for STR profiling to clarify the link between the cells and the primary tumor tissue.

Cell proliferation experiment

CHC-X1 cells from the LGP (P25) were enzymatically dissociated using 0.25% trypsin (VivaCell) to create a

single-cell suspension (CS). After measuring the density of CS, cells were placed at 8×10^3, 1×10^4, 1.2×10^4, 1.5×10^4, 1.8×10^4, 2.1×10^4, 2.4×10^4, and 2.8×10^4 cells per well into 9 wells of the 96-well plate (NEST). CCM 2 was used to bring the liquid volume in each well to 100 µL. After 20 h, a CCK8 solution (10% CCK8 [APExBIO] diluted in 90% RPMI-1640 [Gibco]) was introduced to each well at 100 µL. After 3.5 h, absorbance readings were procured at 450 nm utilizing an enzyme-linked immunosorbent assay (BioTek, synergy H1). Subsequently, a standard curve was generated, plotting absorbance values on the x-axis against corresponding cell counts on the y-axis. The cell doubling time was calculated based on the growth curve, using the website https://doublingtime.com/.

Karyotyping

CHC-X1 cells from the LGP (P35) were harvested, and colchicine (Spectrum) was introduced to the culture medium (CM) to reach a concentration of 0.2 µg/mL. The cells underwent incubation for 90 min and then dissociated into a CS utilizing 0.25% trypsin (Vivacell). After centrifugation, the liquid above was removed and the solid residue was reintroduced into a 0.56% KCl solution. Subsequently, the mixture underwent incubation at 37 °C for 30 min. Fixed solution 1 (a mixture of formic acid and glacial acetic acid [formic acid: glacial acetic acid = 3:1]) was added, mixed well, centrifuged, and the supernatant was removed. The pellet was then resuspended with fixed solution 1 to obtain the chromosome suspension. A single droplet of the suspension was deposited on a glass slide and dehydrated in an oven at 80 °C for 3 h. The dried glass slide was digested in trypsin for 1 min, stained in BIOSIC solution for 8 min, and then rinsed with running water. The slide was sealed and examined utilizing 100× oil immersion objective lenses. Karyotype analysis was executed utilizing ImageJ imaging software and the ChromosomeJ plugin.

Tumor sphere formation experiment

CHC-X1 cells from the LGP (P25) underwent ED and centrifugation to isolate the cells, which were subsequently resuspended in a serum-free medium (RPMI-1640 [Gibco] with 1% penicillin–streptomycin [VivaCell]) to create a CS. This suspension was seeded at a concentration of 2×10^5 cells per well in an ultra-low adherence 6-well plate (NEST) and kept in a moisture-controlled environment at 37 °C with 5% CO_2. Half of the CM was exchanged daily, and the development of tumor spheres was monitored using an inverted microscope (Olympus, IX73 + DP74) on Days 5, 9, and 14 post-seeding.

Organoid culture

Matrigel (BD Pharmingen) was dissolved in a 4°C environment. CHC-X1 cells in the LGP (P28) were enzymatically dissociated into a CS, and the cell concentration was modified to 1×10^4/mL. Subsequently, 100 µL of the CS and Matrigel were thoroughly mixed and dropped into a 12-well plate (NEST) and kept at 37 °C for 30 min for dome formation. After dome formation, 2 mL of CCM 2 was introduced to each well. The cultured plate was then placed in a humidified environment at 37 °C and 5% CO_2 for culturing. The CM was changed every three days, and the morphological changes of the organoids were observed utilizing an inverted microscope (Olympus, IX73 + DP74).

Scanning electron microscopy

CHC-X1 cells from the LGP (P33) underwent ED and centrifugation before being seeded onto sterilized cover slips for cultivation. Once the cells occupied approximately two-thirds of the cover slip surface, the CM was removed, and the cover slips were rinsed with PBS (Vivacell). Subsequently, a 2.5% glutaraldehyde fixative solution (Servicebio) was applied, and the cells were fixed at ambient temperature in darkness for half an hour. The prepared specimens were maintained and transported at 4 °C. They were then dispatched to Wuhan Servicebio Biotechnology Co., Ltd. for embedding, staining, and additional processing. Ultimately, the finished slides were examined and imaged utilizing a scanning electron microscope (HITACHI, Regulus 8100).

Transmission electron microscopy

CHC-X1 cells from the LGP (P33) were collected, and the CM was removed. Subsequently, a 2.5% glutaraldehyde fixative (Servicebio) was introduced to preserve the cells for 5 min. Using a cell scraper, the cells were detached from the culture vessel, centrifuged, and the initial fixative was eliminated. Fresh glutaraldehyde fixative was then applied, and the cells were maintained at ambient temperature in darkness for 30 min. The processed specimens were kept and transported at 4 °C. They were delivered to Wuhan Servicebio Biotechnology Co., Ltd. for embedding, ultra-thin sectioning, and staining procedures. Ultimately, the prepared slides were examined and photographed utilizing a transmission electron microscope (HITACHI, HT7800).

Drugs

Gemcitabine was purchased from Jiangsu Haosen Pharmaceutical Group Co., Ltd. and Jiangsu Hengrui Pharmaceutical Co., Ltd. 5-FU was purchased from Shanghai Xudong Haipu Pharmaceutical Co., Ltd., and paclitaxel was purchased from Wuxi Paclitaxel Pharmaceutical Co., Ltd.

Drug sensitivity test

CHC-X1 cells in their LGP (P30) were harvested, and a monodisperse CS was obtained following enzymatic digestion. The concentration of cells in the suspension was subsequently modified to 1.2×10^5/mL. Following complete mixing, 100 μL of the resultant suspension was distributed into separate wells of a 96-well plate (NEST).

Following 24 h, antineoplastic agents were prepared in varying concentrations utilizing CCM 2, and the existing medium was removed from the 96-well plate. The experimental group received diverse concentrations of the drug solutions, while the control group was exposed to a CCM 2. Each group comprised four wells, with 170 μL of either drug solution or CCM 2 added per well. Following 72 h of exposure, the contents of the 96-well plate were discarded. Subsequently, 100 μL of a diluted CCK8 mixture (10% CCK8 [APExBIO] and 90% RPMI-1640 [Gibco]) was introduced to each well, encompassing four blank wells without CS. The plate was then incubated at 37℃ for 3.5 h, followed by absorbance measurement at 450 nm utilizing an enzyme-linked immunosorbent assay (BioTek, synergy H1). Drug dose–response curves were generated and IC_{50} values were determined utilizing GraphPad Prism 8.0.2 software (GraphPad Inc., San Diego, CA, USA). This procedure was conducted in triplicate.

NXG mice

The study utilized female NXG mice, 5–6 weeks old, procured from Changzhou Cavens Experimental Animal Co., Ltd., and housed in the SPF laboratory of Lanzhou University Animal Experimental Center. The design of animal experimental plans aimed to minimize the pain or discomfort of animals to the greatest extent possible. Before the experiment, the animals were kept under laboratory conditions (temperature 23 °C, humidity 50%, 12 h of light and dark cycle each day, with food and water available ad libitum) for 2 weeks to adapt to the laboratory environment. All animals were euthanized with a dose of barbiturate drugs (pentobarbital sodium [Merck] 150 mg/kg intravenous injection) and tissue collection was performed. The Medical Animal Experiment Ethics Committee of the First Hospital of Lanzhou University approved all animal procedures (LDYYLL2022-345).

Experimental study on xenograft tumor formation in NXG mice

CHC-X1 cells within the LGP (P55) underwent ED to form a CS, and the cell density was modified to 1×10^7/mL. The mixed CS was subcutaneously inoculated in the center of the right armpit of three NXG mice at a rate of 0.1 mL per mouse. The weight changes and expansion of transplanted tumors in NXG mice were regularly monitored. Four weeks later, the mice were euthanized, and xenograft tumors were dissected for observation of the liver and lung tissues of the mice. The xenotransplanted tumors were preserved utilizing 4% paraformaldehyde (Servicebio) for subsequent H&E and IHC staining.

H&E staining and IHC staining

CHC-X1 cells from the LGP (P31) underwent ED and were seeded onto sanitized glass slides for cultivation. Following 60 h, the cover glass was rinsed with PBS, subjected to fixation in 4% paraformaldehyde (Servicebio) for 15 min, and air dried, followed by treatment with 0.5% Triton X-100 (MCE) for 20 min for subsequent staining. The original tumor tissue and xenograft tumor were sectioned into 4-μm sections after paraffin embedding. The slices were dried at 60 °C for 5 h before subsequent staining. They were then immersed in hematoxylin for 5 min, differentiated in a hydrochloric acid and alcohol solution for 30 s, and subsequently stained with eosin for 2 min. Lastly, the sections underwent dehydration, clarification, and were sealed using neutral resin.

IHC staining involved dewaxing and rehydration of the slides, which were then immersed in a sodium citrate solution (10 mmol/L, pH = 6.0) and boiled for 90 s for antigen repair. The slides were exposed to a 3% hydrogen peroxide solution at 37 °C for 15 min. Subsequently, 100 μL of normal goat serum was applied dropwise, and the slides were sealed at 37 °C for 15 min. They were then exposed to antibodies such as anti-CK7, anti-CK19, anti-AFP, anti-Alb, anti-Glypican-3, anti-Arg-1, anti-E-cadherin, anti-Vimentin, anti-Ki-67, anti-CEA, and anti-CA19-9 at 37 °C for 12 h. Thereafter, the secondary antibody was added, and the slides were incubated in ambient conditions for 50 min. The antibody brands and dilution ratios are shown in Table 1. Color development was achieved utilizing a DAB staining kit (Dako), after which the slides were washed under flowing water for 5 min. They were then counterstained with hematoxylin, subjected to dehydration utilizing a gradient ethanol series, cleared with xylene, and finally sealed using neutral resin. The prepared slides were examined under an inverted microscope (Olympus, IX73 + DP74).

Results

Establishment and morphological characteristics of the CHC-X1 CL

A cHCC-CCA CL, named CHC-X1, was effectively generated via primary culture and passage culture. The CHC-X1 CL has been cultured for over 20 months, consistently passaged beyond 100 generations, and has been preserved at the China Typical Culture Collection Center (CCTCC NO: C2023377). Under an inverted microscope, CHC-X1 showed adherent growth, presenting a typical epithelioid appearance with loss of contact inhibition between cells. Most cells were irregularly polygonal, with

Table 1 Reagents for IHC staining

	Antibody	Supplier	Catalogue number	Dilution
Primary antibody	Anti -Cytokeratin 7 Mouse mAb	Servicebio, China	GB12225-100	1:100
	Anti -Cytokeratin 19 Mouse mAb	Servicebio, China	GB12197-100	1:200
	Anti-Glypican 3 Rabbit pAb	Servicebio, China	GB115529-100	1:200
	Anti -Arginase 1 Rabbit pAb	Servicebio, China	GB11285-100	1:200
	Anti- alpha 1 Fetoprotein Mouse mAb	Servicebio, China	GB12287-100	1:100
	Anti -Albumin Mouse mAb	Servicebio, China	GB14005-50	1:200
	Anti -Ki67 Mouse mAb	Servicebio, China	GB121141-100	1:500
	Anti -CA19-9 Mouse mAb	MXB, China	MAB-0778	1:200
	Anti -CEA Mouse mAb	MXB, China	MAB-0852	1:200
Secondary antibody	HRP conjugated Goat Anti-Mouse IgG (H+L)	Servicebio, China	GB23301	1:200
	HRP conjugated Goat Anti-Rabbit IgG (H+L)	Servicebio, China	GB23303	1:200

some appearing spindle-shaped, circular, and elliptical. The nucleus was prominent, and multinucleated giant cells were visible (Fig. 1E and F). CHC-X1 can maintain high vitality after recovery, and even after more than 100 passages, the characteristics of the CL can remain stable.

Short tandem repeat sequence analysis

STR analysis confirmed that the STR patterns of CHC-X1 are different from those of all CLs recorded in the Cellosaurus cell bank. At the same time, the STR pattern of CHC-X1 cells was found to be almost identical to that of the original tumor tissue, with a likelihood rate of 8.0754×10^{32} (Fig. 2A). Therefore, CHC-X1 is a novel human-derived CL procured from primitive tumor tissue.

Cell proliferation experiment

CHC-X1 cells can stably proliferate in RPMI-1640 medium containing 10% FBS. The growth curve of CHC-X1 cells was plotted using the CCK8 method, as shown in Fig. 2B, with a population-doubling time of 50.72 h.

Karyotyping

Karyotype analysis of CHC-X1 cells revealed a complex karyotype, with nearly 83% of cells being triploid and nearly 17% being hexaploidy. In addition, there were abnormalities in both chromosomal number and structure. A representative karyotype observed was 70, XXY der (4) rob (13; 14) rob (15; 21) (Fig. 2C).

Tumor sphere formation experiment and organoid culture

CHC-X1 cells can produce a large number of well-structured tumor spheres under low attachment conditions and in serum-free culture media. With time, both the number and size of these tumor spheres increase (Fig. 3A and B). When CHC-X1 cells are inoculated into Matrigel, they can rapidly form tumor-like organs within 10 days. As the cultivation time increases, the size of these organoids gradually increases. Budding growth can also be observed at the edges of the organoids (Fig. 3C and D).

Ultrastructure of CHC-X1

Scanning electron microscopy revealed that CHC-X1 cells are mainly spherical in shape, with numerous sheet-like and filamentous projections extending outward, demonstrating strong invasiveness. Many cell surfaces can also be observed with more outward protruding vesicles (Fig. 4A and B). Under transmission electron microscopy, CHC-X1 cells show large nuclei with noticeable nucleolus edge aggregation. The cytoplasmic components are relatively small, and the cytoplasm is rich in endoplasmic reticulum, ribosomes, and irregularly swollen mitochondria, with more lysosomes visible (Fig. 4C and D).

Drug sensitivity test

The drug sensitivity of CHC-X1 cells to oxaliplatin, 5-fluorouracil, gemcitabine, and paclitaxel was evaluated. The results indicated that CHC-X1 exhibits resistance to oxaliplatin ($IC_{50} = 9.907$) μmol/L (Fig. 5A), 5-fluorouracil ($IC_{50} = 123.9$ μmol/L (Fig. 5B), and gemcitabine ($IC_{50} = 13.22$) μmol/L (Fig. 5C), while demonstrating sensitivity to paclitaxel ($IC_{50} = 0.03107$) μmol/L (Fig. 5D).

Experimental study on xenograft tumor formation in NXG mice

About 1×10^6 CHC-X1 cells were subcutaneously inoculated into NXG mice. Four weeks after inoculation, CHC-X1 cells successfully generated subcutaneous xenograft tumors at a rate of 67% (Fig. 6A–C). Examination of three mice revealed no metastatic sites in their hepatic or pulmonary tissues (Fig. 6D). The body weight curve and the growth curve of the transplanted tumors in the nude mice are shown in Fig. 6E and F.

H&E staining and IHC staining

H&E staining revealed the destruction of normal structural integrity in the liver tissue in the original tumor, and a large number of cells with large nuclei and deep staining were observed in the cancer lesion. Some cells had a relatively large volume, with a relatively central

A

Loci	CHC-X1		CHC-X1 originated tissue		Matching Probability
Amelogenin	X		X	Y	/
D3S1358	15	16	15	16	0.1890
D5S818	11		11		0.1089
D2S1338	18	23	18	23	0.0775
TPOX	11		11		0.0400
CSF1PO	13		13		0.0156
Penta D	14		14		0.0017
Y- Indel	-		1		/
TH01	7	8	7	8	0.0203
vWA	14	17	14	17	0.1050
D7S820	8	12	8	12	0.0533
D21S11	29	30	30		/
Penta E	8		8		0.0000
D10S1248	14	17	14	17	0.0087
D8S1179	11		11		0.0049
D1S1656	16		16		0.0512
D18S51	16		16		0.0256
D12S391	18	20	18	20	0.0733
D6S1043	11	18	11	18	0.0376
D19S433	13	15.2	13	15.2	0.0763
D16S539	10	13	10	13	0.0257
D13S317	12		12		0.0289
FGA	21	24	21	24	0.0552
LR					8.0754×10^{12}

B

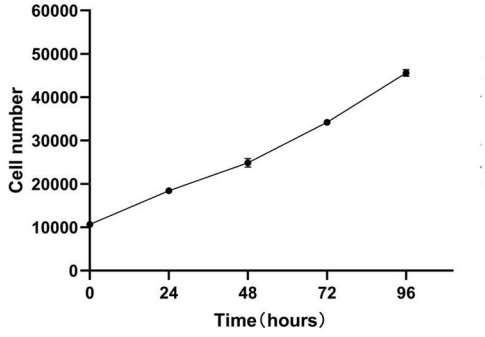

C

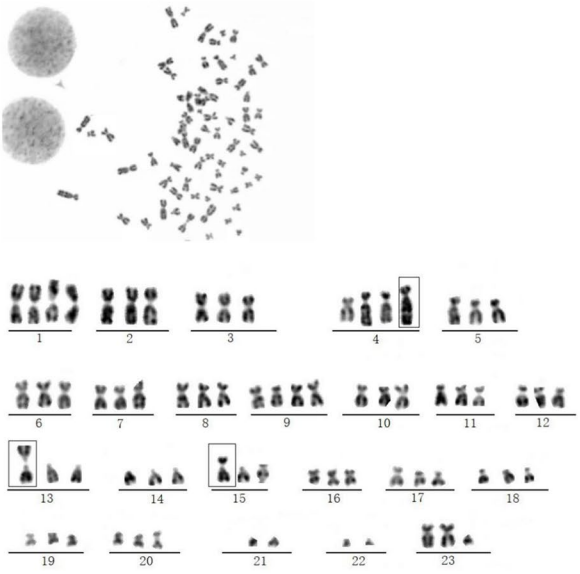

Fig. 2 CHC-X1 cell characteristics. (**A**) Comparative results of short tandem repeat analysis between CHC-X1 cells and the primary tumor; (**B**) Growth curve illustrating the population-doubling time of CHC-X1 cells; (**C**) Karyotype analysis results for CHC-X1 cells, with representative karyotype shown as 70,XXY der(4) rob(13;14) rob(15;21)

nucleus and obvious eosinophilic cytoplasm. The cells were arranged in a fuzzy and coarse, beam-like pattern, morphologically similar to hepatocellular carcinoma (Fig. 7A). Other cells were smaller, with densely stained and significantly deformed nuclei, and a larger nuclear to cytoplasmic ratio. These cells almost completely lost polarity and were arranged in a nest-like pattern, with irregular glandular structures almost invisible. There was loose fibrous stroma between the cells, morphologically similar to poorly differentiated intrahepatic cholangiocarcinoma (Fig. 7B). The two tumor components were mixed with each other and had no clear boundary.

The H&E staining of CHC-X1 cells showed typical characteristics of malignant cells. The cell morphology was diverse, with the majority being polygonal. They showed large and deformed nuclei and obvious nucleoli, and some cells showed a mitotic phase. Multinucleated giant cells could also be seen (Fig. 7C).

H&E staining of the CHC-X1 xenograft tumor suggested that the tumor cells were arranged in a nest-like pattern, forming irregularly-sized glands with abundant interstitial components distributed between glandular ducts. The nucleus was large and round, and the cytoplasm was relatively abundant (Fig. 7D).

IHC staining showed that CK7 (Fig. 8A1–C1), CK19 (Fig. 8A2–C2), AFP (Fig. 8A3–C3), Arg-1 (Fig. 8A5–C5), Alb (Fig. 8A6–C6), and CEA (Fig. 8A10–C10) were all positively expressed in CHC-X1, transplanted tumors, and primary tumors. Glypican-3 (Fig. 8A4–C4) was partially expressed among these three. Ki-67 (Fig. 8A7–C7)

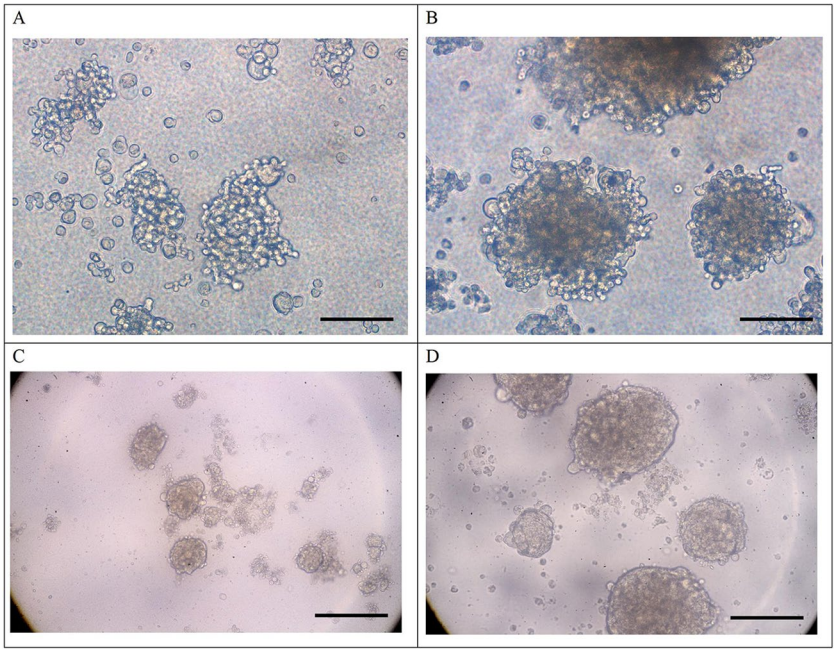

Fig. 3 Tumor sphere and organoid culture. Morphological depiction of CHC-X1 tumor spheres after (**A**) 7 days and (**B**) 14 days (scale bar = 100 μm); Morphological depiction of CHC-X1 cell organoids after (**C**) 4 days and (**D**) 10 days (scale bar = 100 μm)

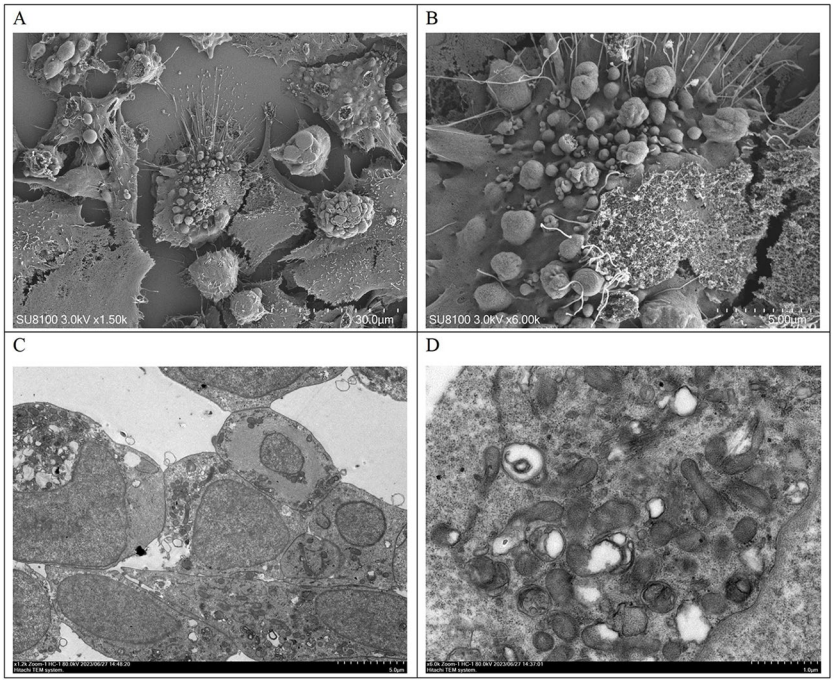

Fig. 4 Ultrastructural examination of CHC-X1 cells using scanning electron microscopy and transmission electron microscopy. (**A** & **B**) CHC-X1 cells are mainly spherical, with numerous sheet-like and filamentous projections extending outward. Many cell surfaces can also be observed with numerous outward protruding vesicles; (**C**) CHC-X1 is mainly circular and elliptical, with a large nucleus and visible nucleolus edge aggregation phenomenon; (**D**) CHC-X1 cells have fewer cytoplasmic components and are rich in endoplasmic reticulum, ribosomes, and irregularly shaped and swollen mitochondria, with more lysosomes visible

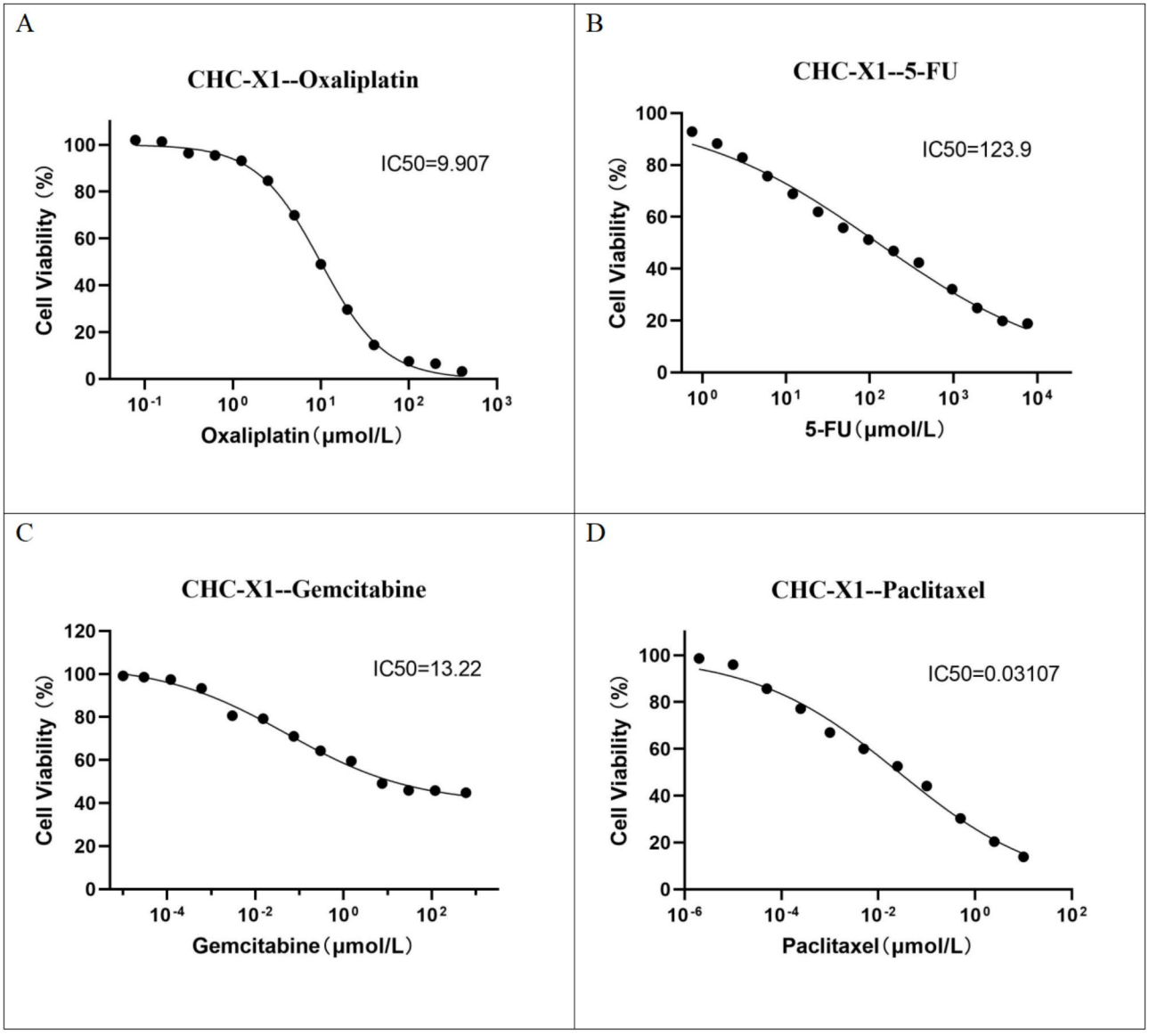

Fig. 5 Assessment of anti-cancer drug sensitivity in CHC-X1 cells. CHC-X1 cells demonstrated resistance to oxaliplatin (**A**), fluorouracil (**B**), and gemcitabine (**C**), and sensitivity to paclitaxel (**D**)

was highly expressed among the three, with an expression rate of approximately 60%. E-cadherin (Fig. 8A8–C8) and Vimentin (Fig. 8A9–C9) were both positively expressed, indicating that CHC-X1 has epithelial–mesenchymal transition characteristics. CA19-9 (Fig. 8A11–C11) was not expressed in any of the three samples. The above findings suggest that CHC-X1 simultaneously expresses IHC markers of both hepatocyte and bile duct cell properties, and to some extent, proves the homology among these three sample types.

Discussion

cHCC-CCA shows high heterogeneity, which is not only reflected within individual tumors but also between different individuals [1, 12, 19, 20]. Many studies have confirmed that the characteristics of the same tumor type and its response to treatment may vary significantly among populations of different regions and ethnicities [21–23]. Therefore, establishing different tumor CLs is crucial for comprehensive research on disease characteristics, exploration, and optimization of treatment plans. In this investigation, we effectively developed an innovative cHCC-CCA CL, CHC-X1. This is the third

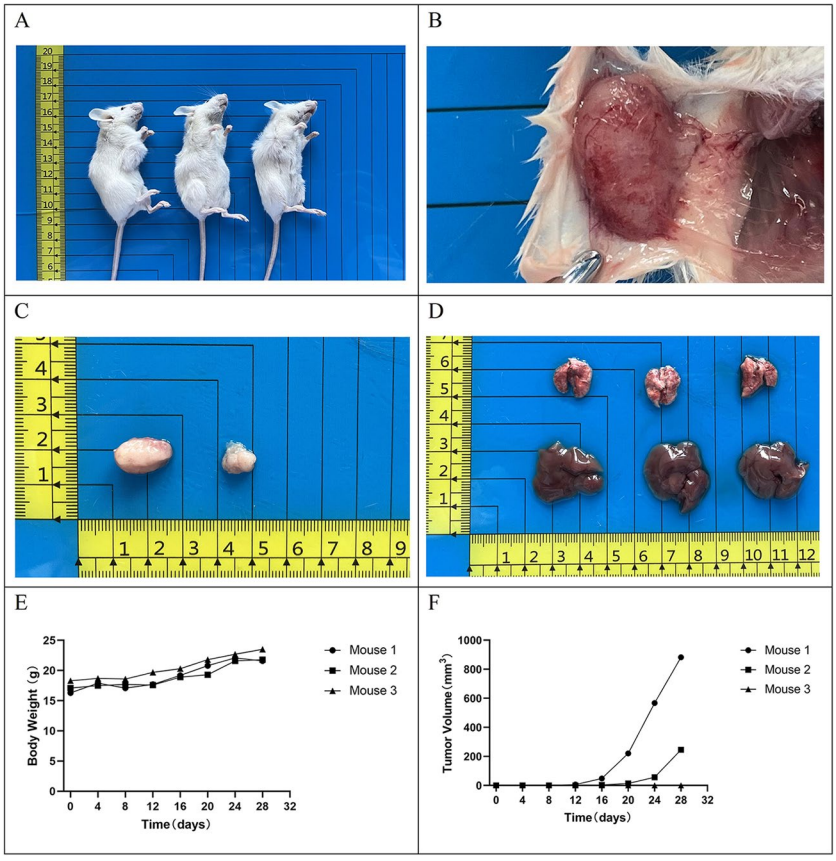

Fig. 6 In vivo studies on xenograft formation by CHC-X1 cells. (**A**–**C**) Subcutaneous transplantation of CHC-X1 cells in nude mice resulted in notable tumor formation (67%); (**D**) No metastatic lesions were observed in the liver and lung tissues of nude mice four weeks after transplantation; (**E** & **F**) Growth curve of the transplanted tumor

cHCC-CCA CL in the world since KMCH-1 and KMCH-2, and also the first cHCC-CCA CL derived from Chinese sources. A comparison of these three CLs is shown in Table 2.

H&E staining is the main method for the pathological diagnosis of cHCC-CCA, and the detection of IHC markers for hepatocellular and cholangiocellular differentiation is an important supplement to H&E staining [24–25]. Markers such as CK7 and CK19 are used to confirm the differentiation components of bile duct cells, while Glypican-3, AFP, Arginase-1, etc. are used to confirm the differentiation components of liver cells [1, 24]. Different degrees of albumin expression are important features of hepatocellular carcinoma [26]. In this study, both hepatocellular carcinoma and poorly differentiated intrahepatic cholangiocarcinoma were identified under H&E staining of the original tumor. The two tumor components were mixed with each other without obvious boundaries, which is consistent with the pathological characteristics of cHCC-CCA. IHC staining confirmed that CHC-X1 cells and primary tumors express both bile duct cell markers such as CK7 and CK19, as well as liver cell markers such as Arg-1, Alb, AFP, and Glypican-3. This IHC analysis also supports the origin of CHC-X1 from cHCC-CCA.

Due to the limited number of clinical cases, there is currently a lack of standardized drug treatment plans for cHCC-CCA. The drugs selected in clinical practice are usually combinations targeting hepatocellular carcinoma and intrahepatic cholangiocarcinoma [1, 27]. Multiple clinical studies have shown that gemcitabine, platinum-based drugs, and 5-FU, either as monotherapy or in combination, have good therapeutic effects on cHCC-CCA, while sorafenib has shown limited therapeutic effects [28–31]. In addition, paclitaxel has been used for the treatment of advanced intrahepatic cholangiocarcinoma and has shown certain effectiveness [32]. Based on this, we evaluated the sensitivity of CHC-X1 cells to oxaliplatin, 5-FU, gemcitabine, and paclitaxel. The results showed that CHC-X1 cells were sensitive to paclitaxel, but showed natural resistance to oxaliplatin, 5-FU, and gemcitabine, which is somewhat different from previously reported clinical studies. Using the differences in drug sensitivity between CHC-X1 cells and other CLs such as KMCH-1 (sensitive to gemcitabine, $IC_{50} = 0.0089$) μmol/L [33], and KMCH-2, we aim to identify potential

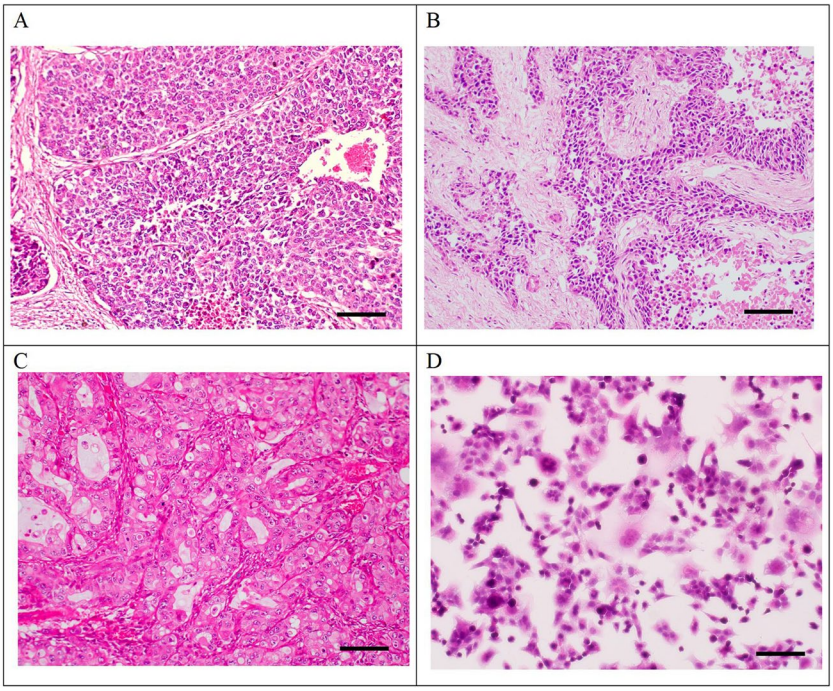

Fig. 7 Hematoxylin and eosin (H&E) staining of primary tumor, xenografted tumor, and CHC-X1 cells. The normal structure of liver tissue is disrupted, and atypical cells are seen inside, arranged in a nest-like or coarse, beam-like pattern, infiltrating and growing. The stroma is rich in blood vessels, and cancer thrombi can be seen in the veins. Morphologically, it is partially similar to hepatocellular carcinoma (**A**) and intrahepatic cholangiocarcinoma (**B**). H&E staining of CHC-X1 xenograft tumor shows that the tumor cells are arranged in a nest-like pattern, forming irregularly sized glands with abundant interstitial components distributed between glandular ducts. The nucleus is large and round, and the cytoplasm is relatively rich (**C**). H&E staining of CHC-X1 cells showed uneven cell morphology, mainly polygonal cells with large and deformed nuclei and obvious nucleoli. In some cells, mitotic phase and multinucleated giant cells were also observed (**D**). (scale bar = 100 μm)

drug resistance-related genes or metabolic pathways in cHCC-CCA. Notably, CHC-X1 cells are naturally resistant to gemcitabine, with an IC_{50} of 13.22 μmol/L, providing a unique perspective in this area of research.

Weems et al. found that melanoma cells can form vesicles (small hemispherical cytoplasmic membrane protrusions on the cell surface), thereby endowing themselves with the ability to resist loss of nest apoptosis. Acquisition of resistance to loss of nest apoptosis resistance is a key step for tumor cells to acquire metastatic ability and contribute to the progression of cancer [34]. Scanning electron microscopy revealed many unevenly sized vesicles on the surface of CHC-X1 cells, indicating that CHC-X1 can be used for research on tumor resistance to loss of nest apoptosis.

Animal models are crucial for in vivo research on tumors [35]. However, not all cell lines can form transplant tumors after inoculation into nude mice [36–38]. Although NXG mice have defects in T cells, B cells, and NK cells, but macrophages and dendritic cells exist normally. CHC-X1 cells can rapidly form transplanted tumors subcutaneously in NXG mice, indicating their possibility for in vivo experimental applications. The formation rate of transplanted tumors is about 67%, which is considered to be related to residual immunity in mice. The uneven size of transplant tumors is a very common phenomenon in transplant tumor research. The reasons for this are considered to be related to tumor cell heterogeneity, errors during inoculation procedures, uneven residual immune function in mice, differences in nutritional status of mice and so on. However, it is difficult to verify the effect of immunotherapy on cHCC-CCA in NXG mice models with severe immune deficiency. Further development and modification of relevant in vivo models are needed to utilize CHC-X1 cells in research related to tumor immunotherapy.

Of course, this study only identified and analyzed the establishment and biological characteristics of a new combined hepatocellular–cholangiocarcinoma cell line CHC-X1, which may limit the universal application of this study in a wider population of CHC patients. The subsequent establishment of more new combined hepatocellular–cholangiocarcinoma cell lines and their sequencing analysis may deepen our understanding of the occurrence, development and the drug resistance mechanism of combined hepatocellular–cholangiocarcinoma.

In summary, we present the development of a novel human combined hepatocellular–cholangiocarcinoma CL, CHC-X1. This new CL offers a fresh experimental platform for investigating the occurrence, developmental

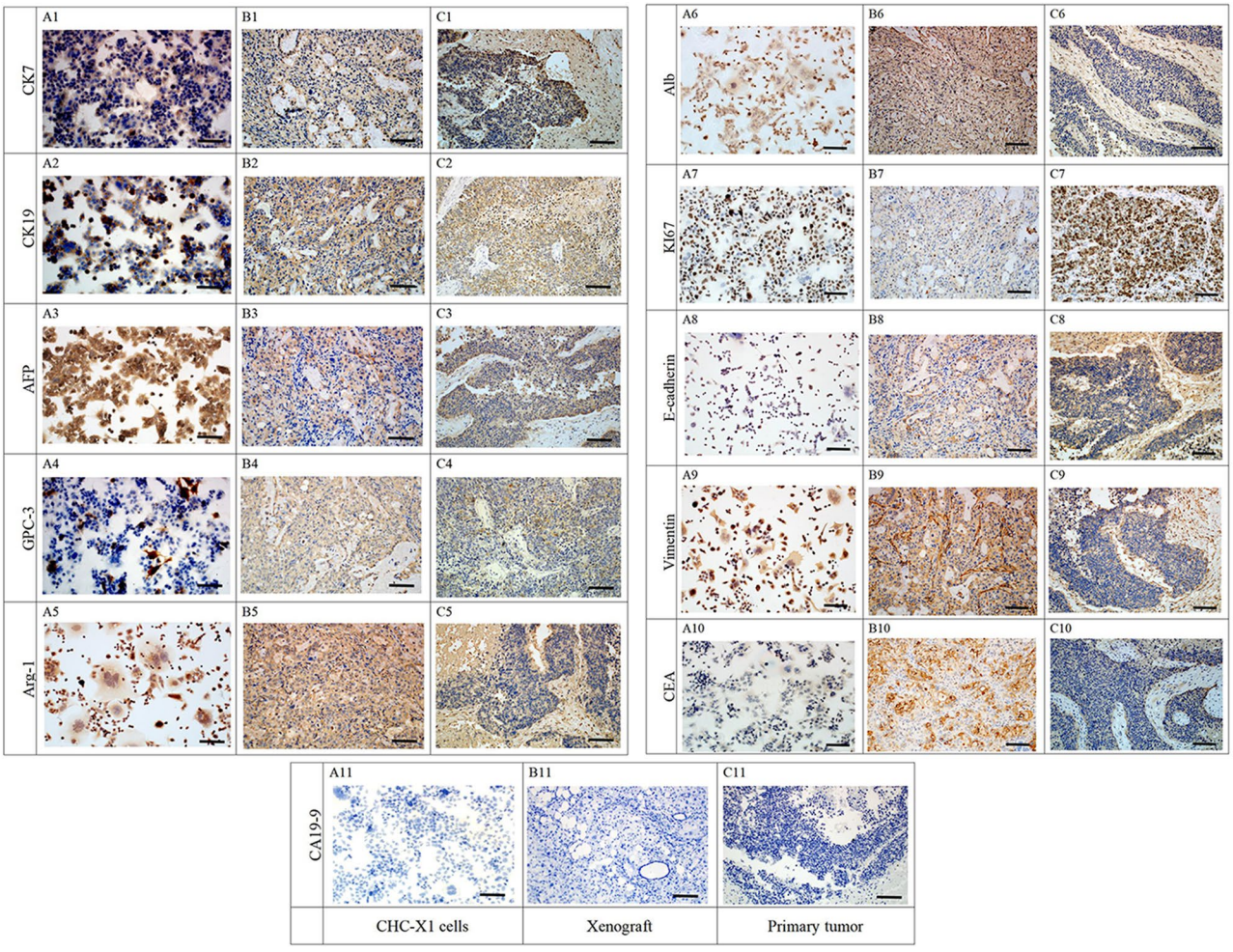

Fig. 8 IHC staining of CHC-X1 cells, xenografted tumor, and primary tumor. (A1), (B1), and (C1) CK7-positive staining in CHC-X1 cells (A1), xenografted tumor (B1), and primary tumor (C1); (A2), (B2), and (C2) CK19-positive staining in CHC-X1 cells (A2), xenografted tumor (B2), and primary tumor (C2); (A3), (B3), and (C3): AFP-positive staining in CHC-X1 cells (A3), xenografted tumor (B3), and primary tumor (C3); (A4), (B4), and (C4) GPC-3-positive staining in CHC-X1 cells (A4), xenografted tumor (B4), and primary tumor (C4); (A5), (B5), and (C5) Arg-1-positive staining in CHC-X1 cells (A5), xenografted tumor (B5), and primary tumor (C5); (A6), (B6), and (C6) Alb-positive staining in CHC-X1 cells (A6), xenografted tumor (B6), and primary tumor (C6); (A7), (B7), and (C7) Quantitative analysis showed a 60% positive rate of Ki67 in CHC-X1 cells (A7), xenografted tumor (B7), and primary tumor (C7); (A8), (B8), and (C8) Positive expression of E-cadherin was observed in CHC-X1 cells (A8), xenografted tumor (B8), and primary tumor (C8); (A9), (B9), and (C9) Positive expression of Vimentin was observed in CHC-X1 cells (A9), xenografted tumor (B9), and primary tumor (C9); (A10), (B10), and (C10) CEA was weakly positive expressed in CHC-X1 cells (A10) and primary tumor (C10); however, positive expression was observed in the xenografted tumor (B10); (A11), (B11), and (C11) Negative expression of CA19-9 was observed in CHC-X1 cells (A11), xenografted tumor (B11), and primary tumor (C11). (scale bar = 50 μm)

Table 2 Summary of cHCC-CCA CLs

	Primary Tumor							Morphology	Doubling Time(h)
	Patient age	Gender	Tumor site	HBV	AFP	CEA	CA19-9		
CHC-X1	31	Male	Left liver	negative	9.3U/ml	943ng/ml	normal	polygon	50.72
KMCH-1	52	Male	Left liver	negative	normal	4.2ng/ml	--	oval	39
KMCH-2	40	Male	Right liver	negative	29ng/ml	2.3ng/ml	317U/ml	polygon	44 (P20) 32 (P55)

	IC_{50}				Tumor Markers					
	Oxaliplatin	Gemcitabine	5-FU	Paclitaxel	CK7	CK19	AFP	Glypican3	Arginase1	Albumin
CHC-X1	9.907μmol/L	13.22μmol/L	123.9μmol/L	0.03107μmol/L	positive	positive	positive	positive	positive	positive
KMCH-1	--	0.0089μmol/L	--	>1μmol/L	positive	positive	--	--	--	--
KMCH-2	--	--	--	--	--	positive	--	--	--	positive

mechanisms, and potential new therapeutic approaches for cHCC-CCA.

Acknowledgements
We would like to thank Bullet Edits (http://www.bulletedits.cn) for English language editing of the manuscript.

Author contributions
HT, CC, XM and HX performed the cell culture. HT, CC, XM and YS performed identification of the cell line, and were major contributors in writing the manuscript. CY, JY, ZW, HZ and ZZ analyzed and interpreted the results of the detection of this novel cell line. HT, CC, XM and HX modified the images and were involved in data processing. CY, JY, ZW, HZ and ZZ were responsible for specimen collection. HT, YS, CY, JY and ZW produced the pathological sections. HT, CC, XM, HX, LW and WZ organized the data for all the experiments. HX, WZ and LW conceived and designed and supervised the study. All authors read and approved the final manuscript.

Funding
This work was supported by grants from National Natural Science Foundation of China (Grants 82260555 and 82360510), Natural Science Foundation of Gansu Province (Grants 23JRRA0929 and 23JRRA1601), Lanzhou Science and Technology Plan Project (Grant 2023-2-38), The Fund of The First Hospital of Lanzhou University (Grant ldyyyn2022-12), Chengguan District Science and Technology Plan (Grant 2023SHFZ0018).

Data availability
The datasets used and/or analysed during the current study are available from the corresponding author upon reasonable request.

Declarations

Ethical approval
The study was conducted according to the guidelines of the *Declaration of Helsinki* and approved by the Ethics Committee of the First Hospital of Lanzhou University (LDYYLL2022-345). Informed consent was obtained from the patient. The animal procedures were approved by the Medical Animal Experiment Ethics Committee of the First Hospital of Lanzhou University (LDYYLL2022-345).

Consent for publication
We have obtained consents to publish this paper from all the participants of this study.

Competing interests
The authors declare no competing interests.

Received: 16 August 2024 / Accepted: 6 March 2025
Published online: 14 March 2025

References

1. Beaufrère A, Calderaro J, Paradis V. Combined hepatocellular-cholangiocarcinoma: an update. J Hepatol. 2021;74(5):1212–24.
2. Garancini M, Goffredo P, Pagni F, Romano F, Roman S, Sosa JA, et al. Combined hepatocellular-cholangiocarcinoma: a population-level analysis of an uncommon primary liver tumor. Liver Transpl. 2014;20(8):952–9.
3. Teufel A, Rodriguez I, Winzler C, Kokh D, Ebert MP, Surovtsova I, et al. Clinical characterization of HCC/CCA mixed cancers in a Population-based cohort. J Gastrointestin Liver Dis. 2023;32(2):190–6.
4. Lin J, Zhang H, Yu H, Bi X, Zhang W, Yin J, et al. Epidemiological characteristics of primary liver Cancer in Mainland China from 2003 to 2020: A representative multicenter study. Front Oncol. 2022;12:906778.
5. Iijima H, Kudo M, Kubo S, Kurosaki M, Sakamoto M, Shiina S, et al. Report of the 23rd nationwide follow-up survey of primary liver cancer in Japan (2014–2015). Hepatol Res. 2023;53(10):895–959.
6. Ramai D, Ofosu A, Lai JK, Reddy M, Adler DG. Combined hepatocellular cholangiocarcinoma: A Population-Based retrospective study. Am J Gastroenterol. 2019;114(9):1496–501.
7. Pomej K, Balcar L, Shmanko K, Welland S, Himmelsbach V, Scheiner B, et al. Clinical characteristics and outcome of patients with combined hepatocellular-cholangiocarcinoma-a European multicenter cohort. ESMO Open. 2023;8(1):100783.
8. Gentile D, Donadon M, Lleo A, Aghemo A, Roncalli M, di Tommaso L, et al. Surgical treatment of hepatocholangiocarcinoma: A systematic review. Liver Cancer. 2020;9(1):15–27.
9. Yen CC, Yen CJ, Shan YS, Lin YJ, Liu IT, Huang HY, et al. Comparing the clinicopathological characteristics of combined hepatocellular-cholangiocarcinoma with those of other primary liver cancers by use of the updated world health organization classification. Histopathology. 2021;79(4):556–72.
10. Wakizaka K, Yokoo H, Kamiyama T, Ohira M, Kato K, Fujii Y, et al. Clinical and pathological features of combined hepatocellular-cholangiocarcinoma compared with other liver cancers. J Gastroenterol Hepatol. 2019;34(6):1074–80.
11. Claasen MPAW, Ivanics T, Beumer BR, de Wilde RF, Polak WG, Sapisochin G, et al. An international multicentre evaluation of treatment strategies for combined hepatocellular-cholangiocarcinoma. JHEP Rep. 2023;5(6):100745.
12. Stavraka C, Rush H, Ross P. Combined hepatocellular cholangiocarcinoma (cHCC-CC): an update of genetics, molecular biology, and therapeutic interventions. J Hepatocell Carcinoma. 2018;6:11–21.
13. Domcke S, Sinha R, Levine DA, Sander C, Schultz N. Evaluating cell lines as tumour models by comparison of genomic profiles. Nat Commun. 2013;4:2126.
14. Barretina J, Caponigro G, Stransky N, Venkatesan K, Margolin AA, Kim S, et al. The Cancer cell line encyclopedia enables predictive modelling of anticancer drug sensitivity. Nature. 2012;483(7391):603–7.
15. Murakami T, Yano H, Maruiwa M, Sugihara S, Kojiro M. Establishment and characterization of a human combined hepatocholangiocarcinoma cell line and its heterologous transplantation in nude mice. Hepatol. 1987; May-Jun;7(3):551–6.
16. Yano H, Iemura A, Haramaki M, Momosaki S, Ogasawara S, Higaki K, et al. A human combined hepatocellular and cholangiocarcinoma cell line (KMCH-2) that shows the features of hepatocellular carcinoma or cholangiocarcinoma under different growth conditions. J Hepatol. 1996;24(4):413–22.
17. Xu H, Miao X, Chai C, Tang H, Hu J, Zhao Z, et al. Establishment and characterization of a new Chinese hepatocellular carcinoma cell line, Hep-X1. Hum Cell. 2023;36(1):434–45.
18. Miao X, Hu J, Chai C, Tang H, Zhao Z, Luo W, et al. Establishment and characterization of a new intrahepatic cholangiocarcinoma cell line derived from a Chinese patient. Cancer Cell Int. 2022;22(1):418.
19. Sciarra A, Park YN, Sempoux C. Updates in the diagnosis of combined hepatocellular-cholangiocarcinoma. Hum Pathol. 2020;96:48–55.
20. De Vito C, Sarker D, Ross P, Heaton N, Quaglia A. Histological heterogeneity in primary and metastatic classic combined hepatocellular-cholangiocarcinoma: a case series. Virchows Arch. 2017;471(5):619–29.
21. Shi Y, Au JS, Thongprasert S, Srinivasan S, Tsai CM, Khoa MT, et al. A prospective, molecular epidemiology study of EGFR mutations in Asian patients with advanced non-small-cell lung cancer of adenocarcinoma histology (PIONEER). J Thorac Oncol. 2014;9(2):154–62.
22. Wang J, Sun Y, Bertagnolli MM. Comparison of gastric cancer survival between Caucasian and Asian patients treated in the united States: results from the surveillance epidemiology and end results (SEER) database. Ann Surg Oncol. 2015;22(9):2965–71.
23. Lin SJ, Gagnon-Bartsch JA, Tan IB, Earle S, Ruff L, Pettinger K, et al. Signatures of tumour immunity distinguish Asian and non-Asian gastric adenocarcinomas. Gut. 2015;64(11):1721–31.
24. WHO Classification of Tumours Editorial Board. WHO classification of tumours. Digestive system tumours. 5th ed. Lyon: IARC; 2019. pp. 260–2.
25. Brunt E, Aishima S, Clavien PA, Fowler K, Goodman Z, Gores G, et al. cHCC-CCA: consensus terminology for primary liver carcinomas with both hepatocytic and cholangiocytic differentation. Hepatology. 2018;68(1):113–26.
26. Ohguchi S, Nakatsukasa H, Higashi T, Ashida K, Nouso K, Ishizaki M, et al. Expression of alpha-fetoprotein and albumin genes in human hepatocellular carcinomas: limitations in the application of the genes for targeting human hepatocellular carcinoma in gene therapy. Hepatology. 1998;27(2):599–607.
27. Schizas D, Mastoraki A, Routsi E, Papapanou M, Tsapralis D, Vassiliu P, et al. Combined hepatocellular-cholangiocarcinoma: an update on epidemiology, classification, diagnosis and management. Hepatobiliary Pancreat Dis Int. 2020;19(6):515–23.
28. Trikalinos NA, Zhou A, Doyle MBM, Fowler KJ, Morton A, Vachharajani N, et al. Systemic therapy for combined Hepatocellular-Cholangiocarcinoma: A Single-Institution experience. J Natl Compr Canc Netw. 2018;16(10):1193–9.

29. Kobayashi S, Terashima T, Shiba S, Yoshida Y, Yamada I, Iwadou S, et al. Multicenter retrospective analysis of systemic chemotherapy for unresectable combined hepatocellular and cholangiocarcinoma. Cancer Sci. 2018;109(8):2549–57.
30. Rogers JE, Bolonesi RM, Rashid A, Elsayes KM, Elbanan MG, Law L, et al. Systemic therapy for unresectable, mixed hepatocellular-cholangiocarcinoma: treatment of a rare malignancy. J Gastrointest Oncol. 2017;8(2):347–51.
31. Salimon M, Prieux-Klotz C, Tougeron D, Hautefeuille V, Caulet M, Gournay J, et al. Gemcitabine plus platinum-based chemotherapy for first-line treatment of hepatocholangiocarcinoma: an AGEO French multicentre retrospective study. Br J Cancer. 2018;118(3):325–30.
32. Shroff RT, Javle MM, Xiao L, Kaseb AO, Varadhachary GR, Wolff RA, et al. Gemcitabine, cisplatin, and nab-Paclitaxel for the treatment of advanced biliary tract cancers: A phase 2 clinical trial. JAMA Oncol. 2019;5(6):824–30.
33. Yamada D, Kobayashi S, Wada H, Kawamoto K, Marubashi S, Eguchi H, et al. Role of crosstalk between interleukin-6 and transforming growth factor-beta 1 in epithelial-mesenchymal transition and chemoresistance in biliary tract cancer. Eur J Cancer. 2013;49(7):1725–40.
34. Weems AD, Welf ES, Driscoll MK, Zhou FY, Mazloom-Farsibaf H, Chang BJ, et al. Blebs promote cell survival by assembling oncogenic signalling hubs. Nature. 2023;615(7952):517–25.
35. Massa A, Varamo C, Vita F, Tavolari S, Peraldo-Neia C, Brandi G, et al. Evolution of the experimental models of cholangiocarcinoma. Cancers (Basel). 2020;12(8):2308.
36. Shultz LD, Goodwin N, Ishikawa F, Hosur V, Lyons BL, Greiner DL. Human cancer growth and therapy in immunodeficient mouse models. Cold Spring Harb Protoc. 2014;2014(7):694–708.
37. Shultz LD, Lyons BL, Burzenski LM, Gott B, Chen X, Chaleff S, et al. Human lymphoid and myeloid cell development in NOD/LtSz-scid IL2R gamma null mice engrafted with mobilized human Hemopoietic stem cells. J Immunol. 2005;174(10):6477–89.
38. Chai C, Tang H, Miao X, Chen T, Su Y, Li L, et al. Establishment and characterization of a novel human gallbladder cancer cell line, GBC-X1. Sci Rep. 2024;14(1):21439.

Publisher's note